Particle & Particle Systems Characterization
www.particle-journal.com

Synthesis of Manganese Oxide Microspheres by Ultrasonic Spray Pyrolysis and Their Application as Supercapacitors

*Yinan Zhang, Laura A. Huff, Andrew A. Gewirth, and Kenneth S. Suslick**

Manganese oxide (MnO_2) microspheres are prepared using an ultrasonic spray pyrolysis (USP) process. A mixed solution of potassium permanganate and hydrochloric acid is nebulized into microsized droplets, which are then carried by air flow through a furnace tube. Each microdroplet serves as one microreactor and produces one microsphere. Upon heating, $KMnO_4$ is decomposed into MnO_2 microspheres; this synthetic process can easily be scaled up. Characterization of the MnO_2 microspheres by scanning electron microscopy, transmission electron microscopy, powder X-ray diffraction, Raman spectroscopy, and X-ray photoelectron spectra is described. Different morphologies of MnO_2 microspheres can be controlled by tuning the precursor concentrations (and ratios) and furnace temperatures. Microspheres synthesized at 150 °C give amorphous MnO_2 while synthesis at 500 °C yields crystalline α-MnO_2. The electrochemical properties investigated by cyclic voltammetry give specific capacitance as high as 320 F g^{-1}, demonstrating promising properties as supercapacitors. In addition, these microspheres can be directly sprayed on conductive substrates, such as carbon fiber paper, and may have useful applications as a supercapacitor electrode coating. The supercapacitive properties of MnO_2 microspheres at higher charge and discharge rates can be improved by increasing the surface area coverage or coating them with a thin layer of conductive polymer.

1. Introduction

Manganese oxide (MnO_2)[1–5] has been widely studied as a promising supercapacitor[6–11] material because it has a high theoretical specific capacitance, low cost, good natural abundance, and is environmentally benign. Substantial efforts have been undertaken to synthesize MnO_2-based nanomaterials with very high surface area in order to maximize the capacitance with high charge/discharge rates. MnO_2 nanomaterials that have been synthesized include nanorods/nanowires,[12,13] nanostructured films,[14] and composite nanomaterials (e.g., with CNT (carbon nanotubes),[15] graphene,[16,17] conductive polymers,[18–20] or metals.[21,22]

Y. Zhang, L. A. Huff, Prof. A. A. Gewirth, Prof. K. S. Suslick
Department of Chemistry
University of Illinois at Urbana Champaign
Urbana, IL 61801, USA
E-mail: ksuslick@illinois.edu

DOI: 10.1002/ppsc.201500061

Other studies report on the synthesis of MnO_2 microspheres and their composites via solution-based processes[23–26] or hydrothermal processes at high temperature.[27–35] Controlling the size and morphology of these MnO_2 microspheres, however, presents a dilemma: control of morphology is difficult without the use of structure-directing agents, but on the other hand, additives such as surfactants may harm the electrochemical properties of the final products. Sub-micronsized spheres are an important class of materials due to their high surface area, good ability to retain high dispersity (i.e., limited aggregation), and excellent processability even without the use of surfactants. MnO_2 microspheres of micron or submicrometer size, however, have been explored only to a limited extent, and only rarely reported as supercapacitor electrode materials.[1,34]

Ultrasonic spray pyrolysis (USP) has been used to prepare a variety of materials including carbon, metal, metal oxides, and semiconductors.[36–41] Carbon microspheres specifically prepared by USP have found several applications for energy storage materials, including supercapacitors and lithium ion batteries.[42–48] Spray processing has also been widely used in industry for fine powder production and thin film deposition because the process is simple and can easily be scaled-up for mass production.[37,40]

In this paper, we introduce a facile and continuous synthesis of MnO_2 microspheres by USP, a fast and scalable methodology.[40] This method specifically avoids the addition of template, surface capping agents, or surfactants (e.g., poly(ethylene glycol) (PEG), oleic acid, polyacrylamide, or citric acid), which can have detrimental consequences for electrochemical properties, but which are essential for solution-based methods. In addition, we find that USP provides a direct route to spray-coating of MnO_2 microspheres directly onto a conductive substrate (i.e., conductive carbon fiber paper), which provides an easy method for the rapid fabrication of supercapacitor electrode materials.

The MnO_2 microspheres formed by USP upon heating nebulized microdroplets containing $KMnO_4$ and HCl. Different morphologies/crystallinity of MnO_2 microperes can be controlled by tuning precursor concentrations and furnace temperatures. Detailed mechanisms are proposed and discussed. The

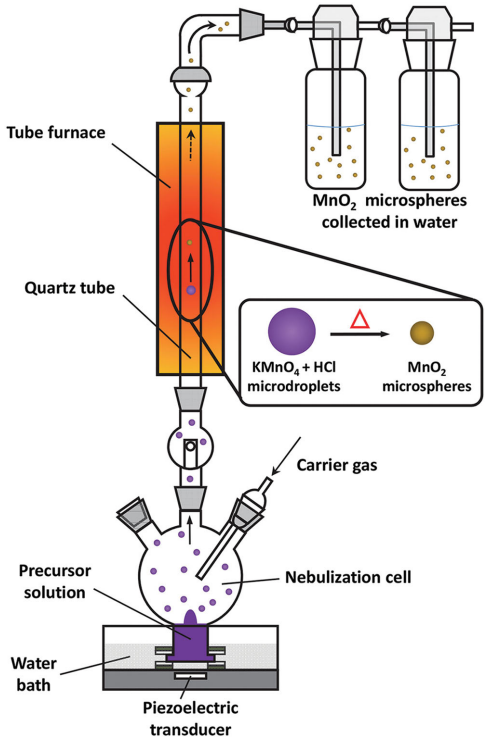

Figure 1. USP apparatus for the synthesis of MnO_2 microspheres.

sub-micron microspheres (diameters from 100 to 1000 nm) made by USP are mesoporous with high surface areas and exhibit the surface area advantages of nanomaterials, while maintaining the easy processability of larger sized powders, even without use of any surfactants. Optimized conditions yield MnO_2 microspheres that exhibit excellent electrochemical properties (e.g., specific capacitances of 320 F g^{-1}), demonstrating a promising route to supercapacitor electrode materials. Finally, we report the improvement of supercapacitive properties of MnO_2 microspheres at higher charge and discharge rates both by increasing their surface area, or by coating them with a thin layer of conductive polymer.

2. Results and Discussion

2.1. MnO_2 Microsphere Formation Mechanism and Characterization

Figure 1 depicts a typical USP apparatus for the synthesis of MnO_2 microspheres. The precursor aqueous solution contains $KMnO_4$ and HCl at different concentrations, which is nebulized into micron-sized droplets and carried by an air flow through the furnace tube. Each droplet serves as a single microreactor, and upon heating, the precursors in the droplet decompose into MnO_2 microspheres. These microspheres are then collected in bubblers as a suspension in water.

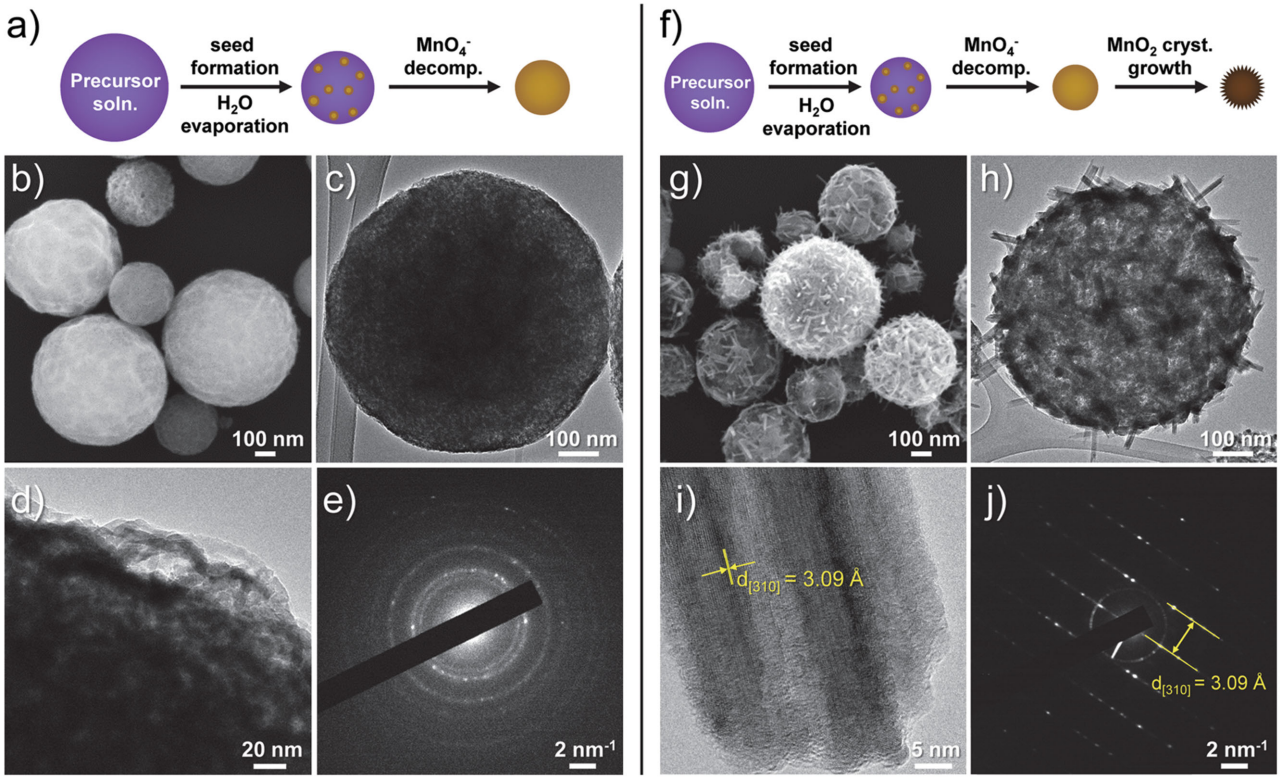

Figure 2. MnO_2 microsphere (synthesized with 100×10^{-3} M $KMnO_4$ and 500×10^{-3} M HCl) formation mechanisms at a) 150 °C and f) 500 °C. SEM images of purified MnO_2 microspheres synthesized at b) 150 °C and g) 500 °C. TEM images of purified MnO_2 microspheres synthesized at c,d) 150 °C and h,i) 500 °C. Electron diffraction patterns of products from e) 150 °C and j) 500 °C.

Part. Part. Syst. Charact. **2015**,
DOI: 10.1002/ppsc.201500061

The morphology of the MnO_2 microspheres can be controlled by varying the ratios of $KMnO_4$:HCl, as well as by tuning the furnace temperature (**Figure 2**). In a typical synthesis, a mixture of 100×10^{-3} M $KMnO_4$ and 500×10^{-3} M HCl is nebulized into microdroplets and heated to 150 °C in the cylindrical furnace. The decomposition of MnO_4^- in acidic media is shown in Reaction R1 below.[49] The reaction is self-catalytic, i.e., MnO_2 seeds initially formed in the droplet will further catalyze additional acidic MnO_4^- to decompose.[32, 50–52]

$$4KMnO_4 + 4HCL \rightarrow 4KCL + 4MnO_2 + 3O_2 + 2H_2O \quad (R1)$$

As illustrated in Figure 2a, the formation of MnO_2 microspheres involves the concentration of the acidic $KMnO_4$ solution as water evaporation occurs, followed by MnO_2 formation upon permanganate decomposition. The spherical shape of MnO_2 microspheres results from the initially isotropic water droplet generated by the ultrasonic nebulization. Scanning electron microscopy (SEM), transmission electron microscopy (TEM), and high-resolution TEM images are given in Figure 2b–d, respectively. Electron beam diffraction indicates a partially amorphous state, as seen in Figure 2e.

In contrast, the reaction pathway of $KMnO_4$ and HCl at 500 °C, shown in Figure 2f–j, produces microspheres made up of MnO_2 nanoneedles that grow on the surface and inside the sphere. The high-resolution TEM (Figure 2i and electron diffraction pattern from the tip of a nanoneedle (Figure 2j) demonstrate that the microspheres are now highly crystalline. The lattice spacing found in the diffraction pattern of 3.09 Å matches with the X-ray powder pattern (d-spacing) of α-MnO_2 with a [310] Miller index. The crystallinity of MnO_2 increases with increasing temperature during USP synthesis (from 150 °C to 300 °C to 500 °C, **Figure 3**). The peaks in the MnO_2 Raman spectra (Figure S1, Supporting Information) match well with previous studies of α-MnO_2.[53,54]

The chemical states and composition of the microspheres' surface were probed by X-ray photoelectron spectra (XPS) analysis (Figure S2, Supporting Information). The Mn peaks, $2p_{3/2}$ (centered at 642 eV) and $2p_{1/2}$ (centered at 653.8 eV), show a spin energy separation of 11.8 eV, which is in good agreement with previously reported MnO_2 data.[15] The Mn to O ratio from the XPS was determined to be 0.5.

When the hydrochloric acid concentration is kept low (between 0 and 50×10^{-3} M), the MnO_4^- (100×10^{-3} M) does not decompose during USP at either 150 °C or 300 °C. At low HCl concentrations, a higher temperature is required to trigger the decomposition of permanganate. Indeed, in the absence of added HCl, a temperature of 500 °C is required to form products. The SEM and TEM images of these products are shown in Figure S3 (Supporting Information). Under USP at 500 °C without added acid, the MnO_2 microspheres are irregular ovals in shape, which implies that the decomposition reaction must occur in the solid state after evaporation of the water (Reaction R2).[55,56] The TEM images (Figure S3b, Supporting Information) show that the MnO_2 crystals grow anisotropically during this process. Upon addition of 50×10^{-3} M HCl, decomposition will occur at 300 °C (and at 500 °C), but again the irregular, non-spherical shape of the products (Figure S4, Supporting Information) shows that the decomposition during USP is still occurring in the solid state.

$$4KMnO_{4(s)} \rightarrow 2K_2O + 4MnO_{2(s)} + 3O_2 \quad (R2)$$

When the precursors are present at higher concentrations (500×10^{-3} to 1000×10^{-3} M $HCl_{(aq)}$ and 100×10^{-3} to 400×10^{-3} M MnO_4^-), the acidified MnO_4^- becomes unstable even at room temperature and spontaneously form seeds of MnO_2 (Reaction R3).[57] Under these conditions, large numbers of MnO_2 seeds form in the solution even before nebulization. Morphologies of MnO_2 microspheres produced under these high concentrations are shown in Figure S5 (Supporting Information). Under high concentration conditions, the MnO_2 microspheres are less porous than those synthesized with lower HCl concentrations, as shown in the TEM images (Figure S5a,b, Supporting Information). At 300 °C, the microspheres begin to collapse and shrink as the amorphous material

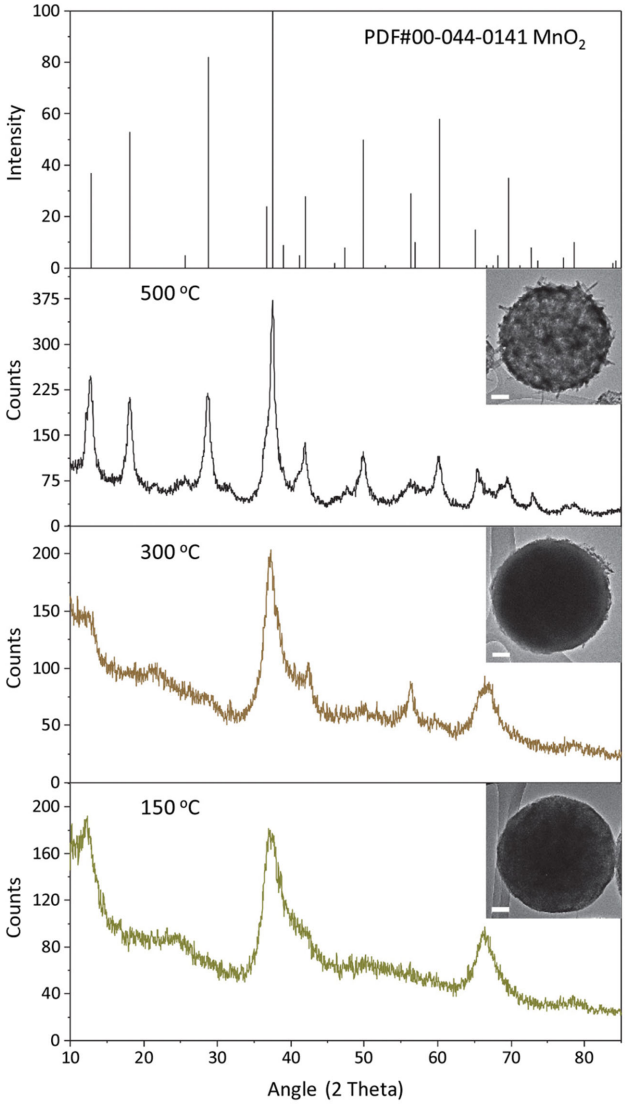

Figure 3. XRD data of MnO_2 microspheres synthesized by USP at different temperatures from an aqueous solution that is 100×10^{-3} M $KMnO_4$ and 500×10^{-3} M HCl. The scale bar is 100 nm.

becomes crystalline. During this process, the MnO_2 surface begins to be decorated by small nanocrystals (Figure S5c,d, Supporting Information). At even higher temperature (500 °C), longer MnO_2 needles grow out from the surface in abundance (Figure S5e,f, Supporting Information).

$$2KMnO_4 + 16HCl \Leftrightarrow 2KCl + 2MnCl_2 + 8H_2O + 5Cl_2 \quad (R3)$$

2.2. Direct Spray of MnO_2 Microspheres for Supercapacitor Electrode Preparation

MnO_2 microspheres formed in the tube furnace are carried forward by the air flow and collected in water inside bubblers for further washing and processing. One may also spray the air-carried MnO_2 microspheres directly onto conductive substrates to form a uniform MnO_2 microsphere coating. **Figure 4**a illustrates the set-up of the spray nozzle over a carbon fiber surface (Spectracarb 2050A-0850, graphitized resin-bonded carbon fiber paper). MnO_2 microspheres are released from the nozzle and sprayed onto the carbon fibers. The coated carbon fibers are allowed to air-dry and subsequently rinsed three times with water to remove any residual impurities. An SEM image taken of uniformly coated carbon paper (Figure 4b) shows fiber-like fine structure thoroughly coated with MnO_2 microspheres. We presume that the adhesion of the MnO_2 microspheres to the carbon fibers is due in part to van der Waals attractions between the microspheres and the fibers and in part to more specific interactions between surface functionality on the carbon (e.g., carboxylates, carbonyls, and alcohol groups) and the MnO_2 surface. In a similar fashion, we have also examined deposition of the MnO_2 microspheres on flat substrates. Figure S6 (Supporting Information) provides an SEM of a flat Si wafer coated with MnO_2 microspheres; the MnO_2 microspheres provide a well-adhered, dense coating to the Si surface.

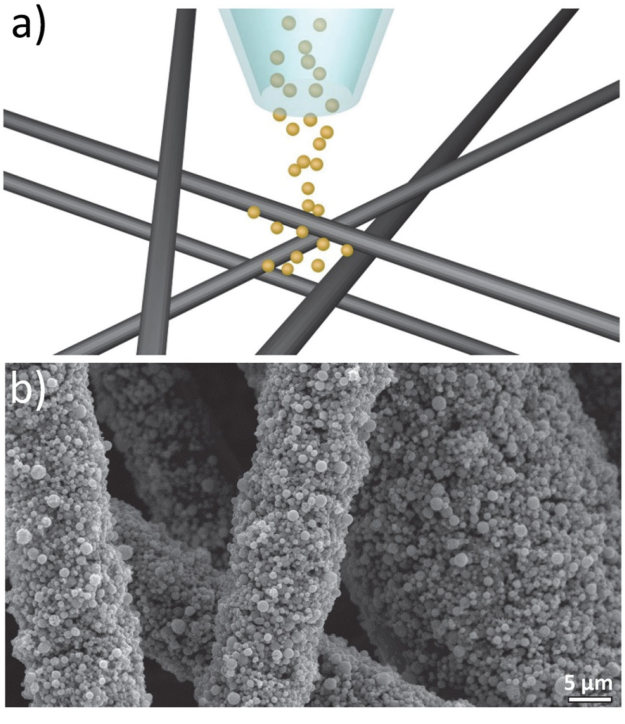

Figure 4. a) Illustration of direct spray of MnO_2 microspheres on carbon fiber paper and b) SEM image of direct spray of MnO_2 microspheres on carbon fiber paper. The MnO_2 microspheres are synthesized from the mixture of 100×10^{-3} M $KMnO_4$ and 500×10^{-3} M HCl at 150 °C.

2.3. Electrochemical Studies of MnO_2 Microspheres

Electrochemical studies were performed on working electrodes prepared by spray-coating conductive carbon fiber paper with MnO_2 microspheres. Cyclic voltammetry (CV) and galvanostatic charge–discharge curves were used to evaluate the supercapacitive properties of MnO_2 microspheres. The MnO_2 microspheres exhibit square shaped CV scans at low scan rates and symmetrical triangular shapes in galvanostatic curves that are indicative of nearly ideal capacitive behavior (Figure S7 and S8, Supporting Information). At high scan rates (>250 mV s^{-1}), however, the CV deviates from the ideal square shape and the specific capacitance drops significantly (**Figure 5**, and Figure S8, Supporting Information). The specific capacitance

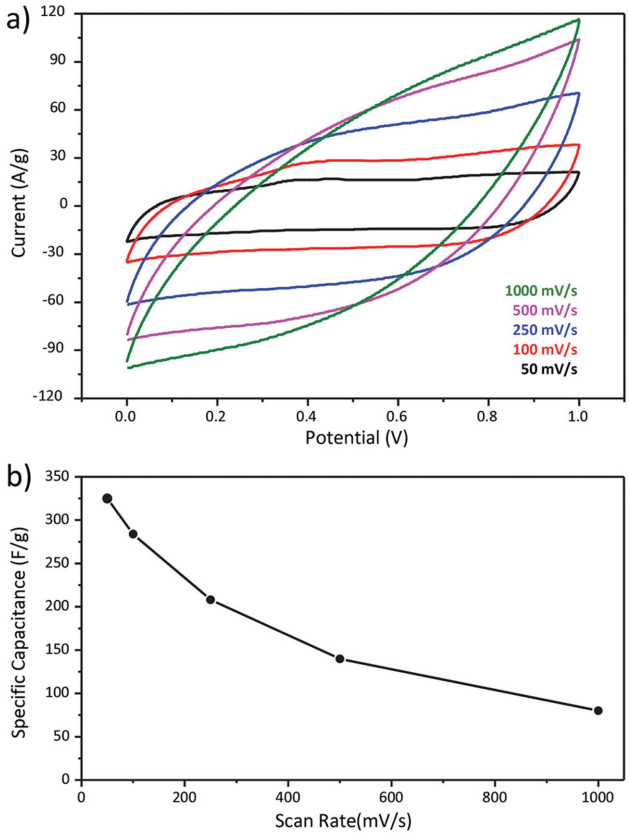

Figure 5. a) Cyclic voltammetry (CV) as a function of scan rate. The CVs exhibit non-ideal capacitive behavior (i.e., deviation from a square shape) at scan rates greater than 250 mV s^{-1}. b) Calculated specific capacitance vs. charge/discharge current density from galvanostatic charge/discharge measurements. The MnO_2 microspheres were USP synthesized from a nebulized solution (100×10^{-3} M $KMnO_4$ and 500×10^{-3} M HCl) heated to 150 °C. The electrolyte used was 1 M $LiClO_4$ aqueous solution.

Part. Part. Syst. Charact. **2015**,
DOI: 10.1002/ppsc.201500061

can be derived from Equation 1,[58] where I is the charge/discharge current, m is the loading mass of the materials, dV/dt is the slope of galvanostatic charge discharge curves (based on chronopotentiometry method). The energy density and power density at different current densities are also calculated,[59] which is shown in Figure S9 (Supporting Information) (Ragone plot). These MnO_2 microsphere supercapacitors can maintain at least 65% of their energy densities (7.3 W h kg^{-1}) and specific capacitance (210 F g^{-1}) as the power density is increased from 0.3 to 6.1 kW kg^{-1}. Moreover, the materials demonstrated excellent cyclability by maintaining shapes of both cyclic votammograms and galvanostatic charge/discharge curves even after 1000 cycles (Figure S10ab, Supporting Information) with 92% retention of capacity after 1000 cycles.

$$C_{spec} = \frac{I}{m\frac{dV}{dt}} \quad (1)$$

The non-ideal capacitive behavior at high scan rates originates from inefficient charge/discharge of the MnO_2 materials, which is attributed to two main reasons. First, the MnO_2 microspheres are densely packed and this limits the amount of surface area available on which redox reactions may occur. Second, the low conductivity of MnO_2 impedes electron transfer between the MnO_2 surface (i.e., redox species at the surface) and the conductive substrate.[60]

To improve the supercapacitive performance of MnO_2 at high charge/discharge rates, we have taken two different approaches: increasing the porosity of the MnO_2 and coating the MnO_2 with highly conductive polymer. The first approach is meant to increase electrolyte access area per unit weigh and the second approach is intended to enhance the MnO_2 utilization per unit area. Previously studies show that thin layers of MnO_2 coated onto conductive substrates permit increases in the specific capacitance to as high as 1380 F g^{-1}, which is close to theoretical specific capacitance value of MnO_2 expected for a redox process involving one electron per manganese atom.[61] Such extremely thin films, however, have limited practical applications since the electrode surface must be prohibitively large. This problem can be solved with a 3D, high-surface-area conductive substrate coated with a very thin layer of MnO_2. Indeed, recent work by Chen et al. has demonstrated that thin layer of MnO_2 coated on nanoporous gold can reach specific capacitance of 1145 F g^{-1} at a decent charge/discharge rate.[62] The gold electrodes used in that study, however, are prohibitively expensive.

2.4. Size and Porosity Control and Their Effects on Electrochemical Properties

The diameter of a droplet generated by sonication is given by the Lang equation, Equation 2,[63] where D_d is diameter of the droplet, σ is the surface tension, ρ is the density of solution, and f is the transducer frequency.

$$D_d = 0.34\left(\frac{8\pi\sigma}{\rho f^2}\right)^{\frac{1}{3}} \quad (2)$$

The diameter of the product is defined in Equation 3,[64] where D_d is diameter of droplet, D_p is diameter of product, M is molecular weight of solute, ρ_p is density of product, C_s is concentration of solute.

$$D_p = D_d\left(\frac{MC_S}{1000\rho_p}\right)^{\frac{1}{3}} \quad (3)$$

Since changes in both density and surface tension are negligible as the precursor ($KMnO_4$) concentration is increased from 50×10^{-3} to 100×10^{-3} M, the particle size is dependent primarily on the precursor concentration. The average diameter of the microsphere obtained from 100×10^{-3} M $KMnO_4$ is 700 ± 100 nm, and average diameter of the microsphere from 50×10^{-3} M $KMnO_4$ is 430 ± 85 nm, as determined from the SEM images (Figure S11, Supporting Information). The microspheres synthesized at lower concentrations of $KMnO_4$ are smaller and more porous, and are therefore less stable when dispersed as colloidal solution; the zeta potential of the microspheres synthesized from 50×10^{-3} M $KMnO_4$ is −23.3 mV, while that obtained from 100×10^{-3} M $KMnO_4$ is −33.75 mV. The importance of the large magnitude of the zeta potential is that it imparts excellent stability to suspensions of the MnO_2 microspheres.

The high porosity of the MnO_2 microspheres is electrochemically advantageous since a greater MnO_2 surface area per unit weight may be accessed by the electrolyte. Both the CV (**Figure 6**) and specific capacitance of particles formed in

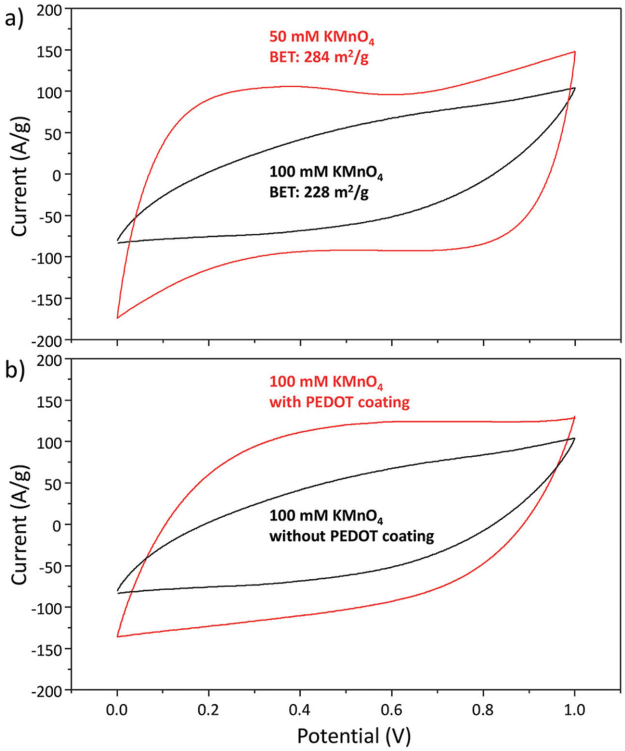

Figure 6. a) Cyclic voltammograms (500 mV s^{-1}) of MnO_2 microspheres synthesized from 100×10^{-3} M and 50×10^{-3} M $KMnO_4$ in 500×10^{-3} M HCl at 150 °C, giving microspheres with different porosity. b) Cyclic voltammograms (500 mV s^{-1}) comparison of MnO_2 microspheres (synthesized from 100×10^{-3} M $KMnO_4$ and 500×10^{-3} M HCl at 150 °C) with and without poly(3,4-ethylenedioxythiophene) (PEDOT) coating.

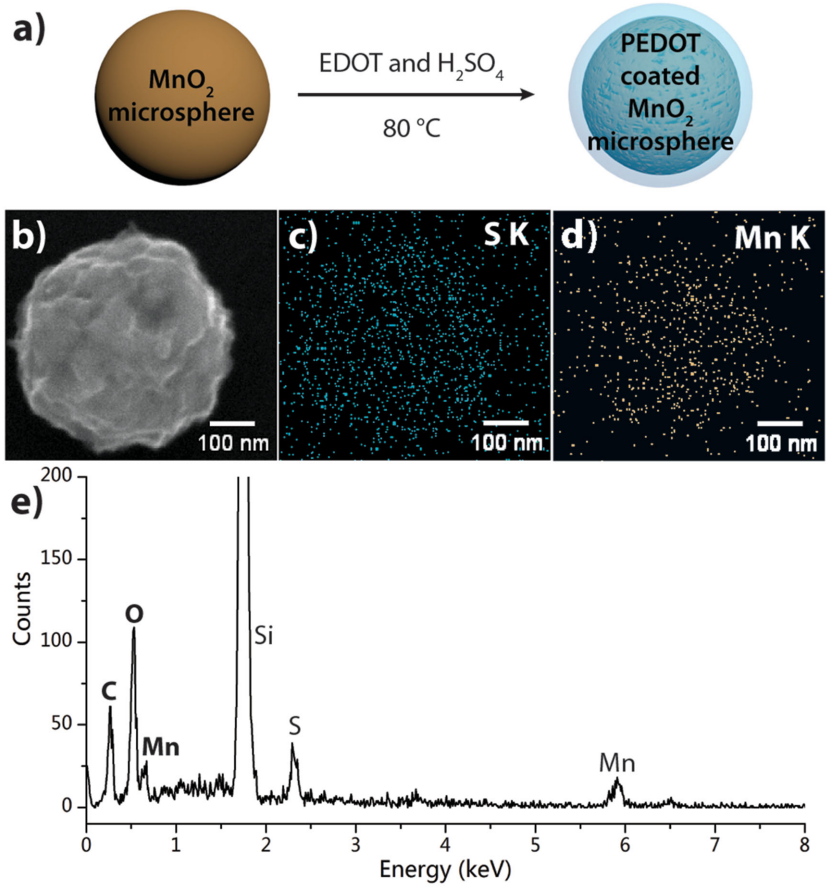

Figure 7. a) Scheme depicting the coating of MnO_2 with PEDOT and b) SEM image of PEDOT-coated MnO_2 microsphere composite. The microsphere here is synthesized via the condition of 100×10^{-3} M $KMnO_4$ and 500×10^{-3} M HCl at 150 °C. c,d) EDX elemental mapping of sulfur and manganese, respectively, of the microsphere composite shown in (b). e) EDX spectra of the whole MnO_2 composite microsphere shown in (b).

50×10^{-3} M $KMnO_4$ precursor (430 nm, BET surface area 284 m^2 g^{-1}) demonstrate increased capacitance compared to those formed in 100×10^{-3} M $KMnO_4$ precursor (700 nm, BET surface area 228 m^2 g^{-1}). These are mesoporous materials, with an average pore dimension of ≈2.0 nm). As expected, the specific capacitance of porous MnO_2 microspheres is also better maintained at high charge discharge rates than less porous microspheres (Figure S12, Supporting Information).

2.5. PEDOT Coating of MnO_2 with Enhanced Electrochemical Properties

As noted above, the problem with MnO_2 is the low conductance that impedes the electrolytes from transporting during realistic charge/discharge rates. Another method to increase capacitance is to coat MnO_2 nanomaterials with a thin layer of highly conductive polymer.[19,20] To this end, we have examined PEDOT as a conductive coating for the MnO_2 microspheres. An SEM image of the PEDOT-coated MnO_2 microspheres is shown in **Figure 7**a, and EDS mappings of the S and Mn elements, respectively, are shown in Figure 7b,c. The EDS mapping indicates that the polymer coats evenly on the MnO_2 microsphere surfaces.

Figure 6b shows cyclic voltammograms at a scan rate of 500 mV s^{-1} of MnO_2 microspheres before and after PEDOT coating. As expected, the specific capacitance of PEDOT-coated MnO_2 microspheres is greater than uncoated MnO_2 microspheres at high charge and discharge rates (Figure S13, Supporting Information). The coating clearly increases the electrochemical kinetics of the MnO_2 microsphere electron transfer due to the high conductivity of the PEDOT coating, which facilitates electron transfer between the shell and MnO_2 core. The PEDOT coating therefore increases the reaction rate per unit area of the MnO_2 microspheres. As a polymer, PEDOT can also improve the mechanical properties of MnO_2, which is normally brittle and fragile, causing the MnO_2 to be more flexible and more easily processed.[19] This is, of course, a compromise: PEDOT has a maximum theoretical supercapacitance of only ≈200 F g^{-1}, which is much lower than that of MnO_2. As a result, the maximum supercapacitance of any composite is inherently lower than pure MnO_2 at infinitely slow scan rates.

3. Conclusion

We have successfully synthesized manganese oxide (MnO_2) microspheres using USP. This process involves thermal decomposition of acidified potassium permanganate in a nebulized micron-sized droplet. The MnO_2 microspheres were thoroughly characterized (SEM, TEM, powder X-ray diffraction (XRD), Raman spectroscopy, and XPS). The morphology and crystallinity of the MnO_2 microspheres can be controlled by tuning precursor concentrations (ratios) and tube furnace temperatures. We also investigate the capacitive properties of MnO_2 microspheres and demonstrate that they are a promising electrode material with applications for supercapacitors since they exhibit a specific capacitance of 320 F g^{-1}. Finally, we have successfully improved the capacitive properties of MnO_2 particles at high charge and discharge rates by increasing the effective surface area and coating with a thin layer of conductive polymer.

This microsphere synthesis method is facile and can easily be scaled up. Importantly, the microspheres can be sprayed directly from the USP apparatus onto a conductive substrate (i.e., conductive carbon fiber paper). This gas-phase spray-coating provides for an easy method of fabrication of supercapacitor electrode materials with high specific capacitances and excellent cyclability.

Part. Part. Syst. Charact. **2015**,
DOI: 10.1002/ppsc.201500061

Particle & Particle Systems Characterization
www.particle-journal.com

Received: May 4, 2015
Revised: May 20, 2015
Published online:

4. Experimental Section

Preparation of MnO_2 Microspheres: The USP set-up is depicted in Figure 1. The operating frequency of the water nebulizer is 1.7 MHz. The furnace was preheated to the desired temperature (e.g., 150 °C). Air was used as the carrier gas at a flow rate of 0.5 L min^{-1}. The precursor solution (100×10^{-3} M $KMnO_4$ and 500×10^{-3} M HCl) was prepared and then immediately added to the nebulizing chamber. The black-brown powders were collected in bubblers containing water and subsequently washed and centrifuged with deionized water a minimum of four times. The final products were dried overnight in a vacuum oven at 100 °C. The as-prepared powders were then used for further characterization.

Synthesis of PEDOT-Coated MnO_2Microspheres: 50 µL of 100×10^{-3} M sodium dodecyl sulfate (SDS) solution was added to 5 mL of 14.8×10^{-3} M 3,4-ethylenedioxythiophene (EDOT) solution. This mixture was then added to 5 mL of 0.25 mg mL^{-1} MnO_2 dispersant (prepared by sonicating as prepared MnO_2 powder in deionized water for 2 min). Next, 25 µL of 1 M H_2SO_4 solution was added to this solution under stirring. The mixture was kept at 80 °C in a water bath under stirring at 500 rpm until its color changed from brown to blue-brown. The reaction was then quenched with ice and the product was collected by centrifugation and washed three times. The product was then drop-cast onto preweighed carbon paper, which was then thoroughly dried under vacuum at room temperature. This coated carbon paper then served as working electrode for electrochemical studies.

Material Characterization: SEM images were taken using a JEOL 7000F field emission (FE)-SEM instrument operated at 10 kV. Energy-dispersive X-ray spectroscopy (EDX) is coupled with the 7000F-SEM instrument using a Thermo Electron EDX microanalysis system. TEM was conducted using a JEOL 2100 Cryo instrument operated at 200 kV. Raman spectroscopy was collected by a Nanophoton RAMAN 11 laser Raman microscope a frequency-doubled Nd:YAG 532-nm laser (laser power 0.267 mW). The Brunauer–Emmett–Teller (BET) specific surface area was measured using a Quantachrome Nova 2200e system. XPS were collected on a Kratos Axis ULTRA instrument (Al K_α radiation). Powder XRD patterns were obtained on a Siemens–Bruker D-5000 XRD instrument operated at 40 kV and 30 mA (Cu K_α radiation). Zeta potential was measured using a zetaPALS zeta potential analyzer.

Electrochemical Experiments: Working electrodes were prepared by directly spraying MnO_2 microspheres onto preweighed carbon paper. The spray-coated carbon paper was then washed thoroughly with deionized water to remove any unreacted precursor species. The spray-coated carbon paper was then dried thoroughly under vacuum, baked at 120 °C, and weighed. The amount of deposited material was then calculated from this weight. The MnO_2 coatings are well-adhered to the carbon paper, and exhaustive washing does not lead to any significant loss of deposited material; similarly after 1000 charge/discharge cycles no significant loss of material is observed. An SEM image of the electrode is shown in **Figure 4**b. The CV and galvanostatic charge/discharge based on chronopotentiometry (CP) were conducted using a CH Instruments Electrochemical Workstation (potentiostat/galvanostat) with a platinum mesh counter electrode and a silver/silver chloride (Ag/AgCl) reference electrode. The measurements were made at five different scan rates (50, 100, 250, 500, and 1000 mV s^{-1}), and at five different current densities (2.5, 5, 10, 25, and 50 mA cm^{-2}), respectively. All electrochemical experiments were conducted in 1 M $LiClO_4$ aqueous solution.

Supporting Information

Supporting Information is available from the Wiley Online Library or from the author.

Acknowledgements

This work was supported by NSF (DMR 12-06355). This research was carried out in part in the Frederick Seitz Materials Research Laboratory Central Research Facilities, University of Illinois.

[1] W. Wei, X. Cui, W. Chen, D. G. Ivey, *Chem. Soc. Rev.* **2011**, *40*, 1697.
[2] C. C. Hu, T. W. Tsou, *Electrochem. Commun.* **2002**, *4*, 105.
[3] M. Toupin, T. Brousse, D. Belanger, *Chem. Mater.* **2002**, *14*, 3946.
[4] R. N. Reddy, R. G. Reddy, *J. Power Sources* **2003**, *124*, 330.
[5] G. Wang, L. Zhang, J. Zhang, *Chem. Soc. Rev.* **2012**, *41*, 797.
[6] B. E. Conway, *J. Electrochem. Soc.* **1991**, *138*, 1539.
[7] R. Kotz, M. Carlen, *Electrochim. Acta* **2000**, *45*, 2483.
[8] A. S. Arico, P. Bruce, B. Scrosati, J. M. Tarascon, W. van Schalkwijk, *Nat. Mater.* **2005**, *4*, 366.
[9] P. Simon, Y. Gogotsi, *Nat. Mater.* **2008**, *7*, 845.
[10] V. Augustyn, P. Simon, B. Dunn, *Energy Environ. Sci.* **2014**, *7*, 1597.
[11] J. Wang, H. L. Xin, D. Wang, *Part. Part. Syst. Charact.* **2014**, *31*, 515.
[12] V. Subramanian, H. W. Zhu, R. Vajtai, P. M. Ajayan, B. Q. Wei, *J. Phys. Chem. B* **2005**, *109*, 20207.
[13] X. Wang, Y. D. Li, *J. Am. Chem. Soc.* **2002**, *124*, 2880.
[14] Y. Omomo, T. Sasaki, L. Z. Wang, M. Watanabe, *J. Am. Chem. Soc.* **2003**, *125*, 3568.
[15] A. L. M. Reddy, M. M. Shaijumon, S. R. Gowda, P. M. Ajayan, *Nano Lett.* **2009**, *9*, 1002.
[16] S. Chen, J. W. Zhu, X. D. Wu, Q. F. Han, X. Wang, *ACS Nano* **2010**, *4*, 2822.
[17] Z. S. Wu, W. C. Ren, D. W. Wang, F. Li, B. L. Liu, H. M. Cheng, *ACS Nano* **2010**, *4*, 5835.
[18] Y. Hou, Y. W. Cheng, T. Hobson, J. Liu, *Nano Lett.* **2010**, *10*, 2727.
[19] R. Liu, S. B. Lee, *J. Am. Chem. Soc.* **2008**, *130*, 2942.
[20] R. Liu, J. Duay, S. B. Lee, *ACS Nano* **2010**, *4*, 4299.
[21] H. Pang, S. Wang, G. Li, Y. Ma, J. Li, X. Li, L. Zhang, J. Zhang, H. Zheng, *J. Mater. Chem. A* **2013**, *1*, 5053.
[22] C. Yuan, L. Zhang, L. Hou, G. Pang, X. Zhang, *Part. Part. Syst. Character.* **2014**, *31*, 778.
[23] J. Ni, W. Lu, L. Zhang, B. Yue, X. Shang, Y. Lv, *J. Phys. Chem. C* **2008**, *113*, 54.
[24] Q. Qu, P. Zhang, B. Wang, Y. Chen, S. Tian, Y. Wu, R. Holze, *J. Phys. Chem. C* **2009**, *113*, 14020.
[25] G.-Q. Zhang, X.-G. Zhang, H.-L. Li, *J. Solid State Electrochem.* **2006**, *10*, 995.
[26] J. P. Hill, S. Alam, K. Ariga, C. E. Anson, A. K. Powell, *Chem. Commun.* **2008**, *3*, 383.
[27] Y. Sun, L. Wang, Y. Liu, Y. Ren, *Small* **2015**, *11*, 300.
[28] M. Liu, L. Gan, W. Xiong, Z. Xu, D. Zhu, L. Chen, *J. Mater. Chem. A* **2014**, *2*, 2555.
[29] M. Kim, J. Kim, *ACS Appl. Mater. Interfaces* **2014**, *6*, 9036.
[30] M. Kim, J. Kim, *Phys. Chem. Chem. Phys.* **2014**, *16*, 11323.
[31] Q. Lu, Y. Zhou, *J. Power Sources* **2011**, *196*, 4088.
[32] R. Chen, J. Yu, W. Xiao, *J. Mater. Chem. A* **2013**, *1*, 11682.
[33] X. Zhou, S. Chen, D. Zhang, X. Guo, W. Ding, Y. Chen, *Langmuir* **2006**, *22*, 1383.
[34] O. Ghodbane, J. L. Pascal, F. Favier, *ACS Appl. Mater. Interfaces* **2009**, *1*, 1130.
[35] W. Y. Ko, L.-J. Chen, Y.-H. Chen, W.-H. Chen, K.-M. Lu, J.-R. Yang, Y.-C. Yen, K.-J. Lin, *J. Phys. Chem. C* **2013**, *117*, 16290.
[36] G. L. Messing, S.-C. Zhang, G. V. Jayanthi, *J. Am. Ceram. Soc.* **1993**, *76*, 2707.
[37] T. Toivo, M. J. H.-S. Kodas, *Aerosol Processing of Materials*, Wiley, New York, **1998**.
[38] K. Okuyama, I. Wuled Lenggoro, *Chem. Eng. Sci.* **2003**, *58*, 537.
[39] J. H. Bang, K. S. Suslick, *Adv. Mater.* **2010**, *22*, 1039.
[40] J. H. Bang, Y. T. Didenko, R. J. Helmich, K. S. Suslick, *Aldrich Mater. Matter* **2012**, *7*, 15.

[41] H. Xu, B. W. Zeiger, K. S. Suslick, *Chem. Soc. Rev.* **2013**, *42*, 2555.
[42] H. Kim, M. E. Fortunato, H. Xu, J. H. Bang, K. S. Suslick, *J. Phys. Chem. C* **2011**, *115*, 20481.
[43] H. Xu, J. Guo, K. S. Suslick, *Adv. Mater.* **2012**, *24*, 6028.
[44] B. Jokić, S. Drmanić, T. Radetic, J. Krstić, R. Petrović, A. Orlović, D. Janaćković, *Mater. Lett.* **2010**, *64*, 2173.
[45] S. E. Skrabalak, *Phys. Chem. Chem. Phys.* **2009**, *11*, 4930.
[46] D. S. Jung, T. H. Hwang, J. H. Lee, H. Y. Koo, R. A. Shakoor, R. Kahraman, Y. N. Jo, M. S. Park, J. W. Choi, *Nano Lett.* **2014**, *14*, 4418.
[47] L. Q. Mai, A. Minhas-Khan, X. Tian, K. M. Hercule, Y. L. Zhao, X. Lin, X. Xu, *Nat. Commun.* **2013**, *4*, 2923.
[48] Y. N. Ko, S. B. Park, K. Y. Jung, Y. C. Kang, *Nano Lett.* **2013**, *13*, 5462.
[49] D. Y. Li, Y. F. Chen, *Mater. Sci. Forum* **2011**, *688*, 107.
[50] J. Wang, J. Liu, Y. Zhou, P. Hodgson, Y. Li, *RSC Adv.* **2013**, *3*, 25937.
[51] W. Xiao, D. Wang, X. W. Lou, *J. Phys. Chem. C* **2009**, *114*, 1694.
[52] H. G. Byers, *A Study of the Reduction of Permanganic Acid by Manganese Dioxide*, The Chemical Publishing Company, London, UK **1899**.
[53] T. Gao, H. Fjellvåg, P. Norby, *Anal. Chim. Acta* **2009**, *648*, 235.
[54] C. Julien, *Solid State Ionics* **2003**, *159*, 345.
[55] F. Herbstein, G. Ron, A. Weissman, *J. Chem. Soc. A* **1971**, 1821.
[56] F. Herbstein, M. Kapon, A. Weissman, *J. Therm. Anal.* **1994**, *41*, 303.
[57] F. Venable, D. Jackson, *J. Am. Chem. Soc.* **1920**, *42*, 237.
[58] M. M. Shaijumon, F. S. Ou, L. Ci, P. M. Ajayan, *Chem. Commun.* **2008**, *20*, 2373.
[59] J. P. Zheng, *J. Electrochem. Soc.* **2005**, *152*, A1864.
[60] J. K. Chang, W. T. Tsai, *J. Electrochem. Soc.* **2003**, *150*, A1333.
[61] M. Toupin, T. Brousse, D. Bélanger, *Chem. Mater.* **2004**, *16*, 3184.
[62] X. Lang, A. Hirata, T. Fujita, M. Chen, *Nat. Nanotechnol.* **2011**, *6*, 232.
[63] R. J. Lang, *J. Acoust. Soc. Am.* **1962**, *34*, 6.
[64] A. Gurav, T. Kodas, T. Pluym, Y. Xiong, *Aerosol Sci. Technol.* **1993**, *19*, 411.

Part. Part. Syst. Charact. **2015**,
DOI: 10.1002/ppsc.201500061